Supplementary information to:

Synergistic effects boosting hydrogen evolution performance of transition metal oxides at ultralow Ru loading

Miao Yang,*[a] Hong Yang,[a] Feng Wang,[a] Yulan Niu*[a] and Pan Li *[b]

[a] Collaborative Innovation Center of CO_2 Conversion and Utilization, Department of Chemistry and Chemical Engineering, Taiyuan Institute of Technology, Taiyuan Shanxi, 030008, PR China

E-mail: m_miaoyang@163.com; niuyl@tit.edu.cn

[b] Department of Environment and Safety Engineering, Taiyuan Institute of Technology, Taiyuan Shanxi, 030008, PR China

E-mail: lipan201104@163.com

Experimental Section

Materials

KOH (AR, ⩾85%), HCl (AR, 36.0～38.0%), and Ethanol (AR, ⩾95%) were sourced from Sinopharm Chemical Reagent Co., Ltd. $Ni(NO_3)_2 \cdot 6H_2O$ (AR, 98%), Na_2MoO_4 (AR, 99%), and $RuCl_3$ (Ru content 45~55%) were purchased from Aladdin (Shanghai, China). All the reagents were used without any further purification.

Synthesis of Ru-$NiMoO_4$/NF

In a typical preparation of the Ru-$NiMoO_4$/NF, one piece of commercial Nickel Foam (NF) was cleaned in HCl, ethanol, and DI water by ultrasonic to remove the oxide layer. The cleaned NF was placed in the hydrothermal synthesis reactor with the same mole ratio of Na_2MoO_4 and $Ni(NO_3)_2 \cdot 6H_2O$ aqueous solution. Then, the hydrothermal synthesis reactor was sealed and heated at 150^oC for 6 hour. After cooling to room temperature, the $NiMoO_4$/NF precursor was obtained after washed with DI water and ethanol. Then, the obtained $NiMoO_4$/NF precursor was immersed into ethanol solution containing $RuCl_3$ and heated at 100^oC for 12 h. Finally, the sample was placed in a porcelain boat and annealed at 350 ^oC for 2 h in N_2 atmosphere with the heating rate of 2 min^{-1} to synthesis Ru-$NiMoO_4$/NF. The mass of the Ru-$NiMoO_4$/NF and $NiMoO_4$/NF are 6.3 mg cm^{-2} and 13.7 mg cm^{-2}, respectively.

Preparation of Ru+$NiMoO_4$/NF

Briefly, 10 mg of 5 wt.% commercial Ru/C catalyst was dispersed into a solution (40 μL ethanol, 50 μL water, and 10 μL 5% Nafion) and sonicated for 30 min to obtain a uniform ink solution. Subsequently, 60 μL of the ink solution was dropped on the NF (1 × 1 cm^{-2}) and dried at room temperature.

Material characterizations

Scanning electron microscopy (SEM) measurements were conducted to study the morphology of the samples on ZEISS Sigma 300. High-resolution transmission electron microscopy (HR-TEM) was performed on JEOL JEM 2100F. Inductively coupled plasma optical emission spectrometer (ICP-OES) was obtained from Aglient 7850. The sample was dissolved in the mixed solution of nitric acid and hydrochloric acid. Powder X-ray diffraction (XRD) was carried out on Rigaku Miniflex 600. X-ray photoelectron spectroscopy (XPS) was undertaken on Thermo Scientific K-Alpha. N_2 adsorption-desorption isotherm were recorded by Micromeritics ASAP 2460.

Electrocatalytic measurements

Electrochemical workstation (CHI 760E; Shanghaichenhua Instruments, China) instrument was used to evaluated the electrochemical performance of the catalysts in a standard three-electrode system at room temperature. The as-prepared catalysts cut into 1×1 cm^2 were as working electrode, the graphite rod was as counter electrode, and the Hg/HgO electrode was as reference electrode. All of the electrochemical data were converted to reversible hydrogen electrode (RHE) according to the following Nernst equation: $E(RHE)=E(Hg/HgO)+E^{\ominus}(Hg/HgO)+0.059\times pH$. The Linear sweep voltammetry (LSV) was recorded in 1M KOH with iR compensation at a scan rate of 5 mV s^{-1}. EIS measurements were evaluated in the frequency range from 0.1 Hz to 100 kHz with an amplitude of 5 mV. The stability of Ru-$NiMoO_4$/NF was tested by chronoamperometric i-t measurement.

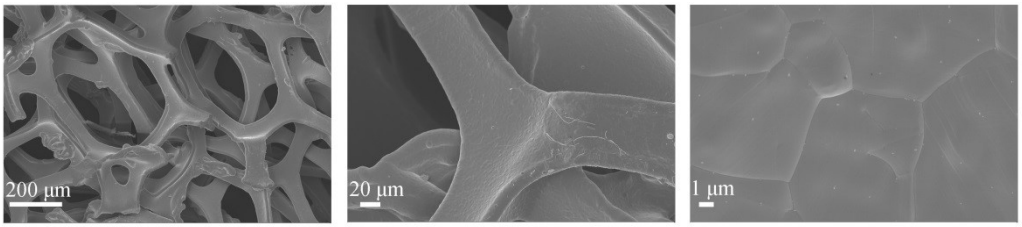

Fig. S1 SEM images of pure NF at different magnifications.

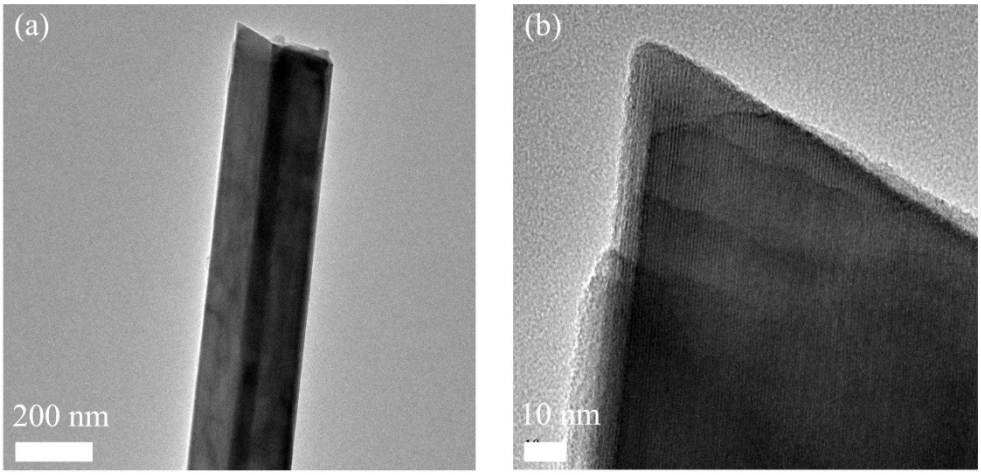

Fig. S2 TEM images of $NiMoO_4$-NF at different magnifications.

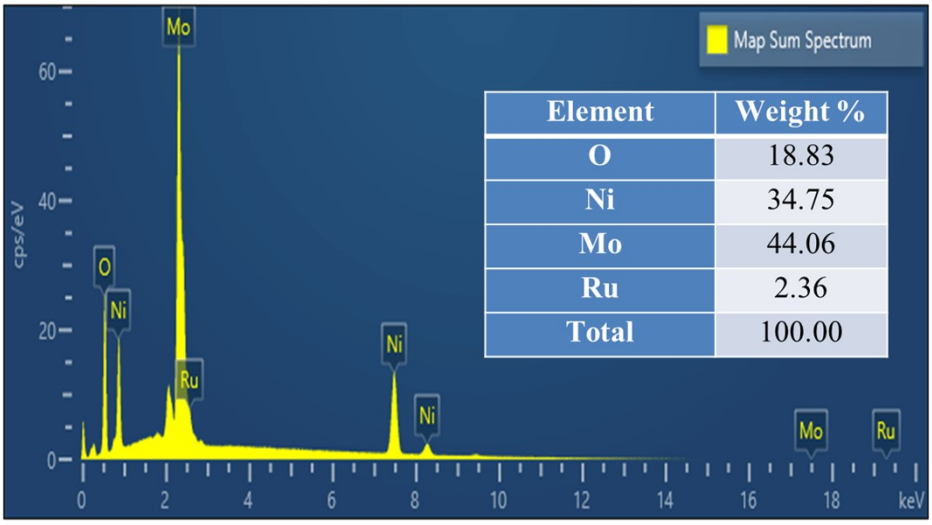

Element	Weight %
O	18.83
Ni	34.75
Mo	44.06
Ru	2.36
Total	100.00

Fig. S3 The EDS spectrum of Ru-$NiMoO_4$-NF.

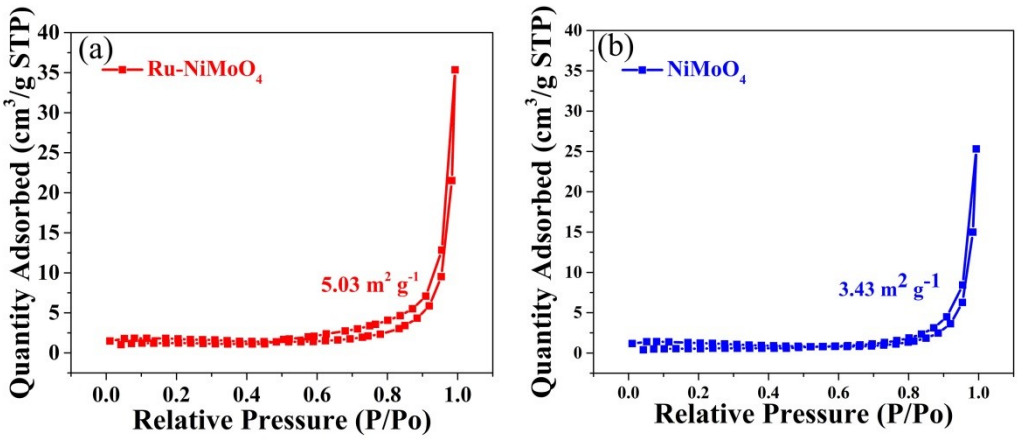

Fig. S4 N_2 adsorption-desorption isotherms of (a) Ru-$NiMoO_4$-NF and (b) $NiMoO_4$-NF.

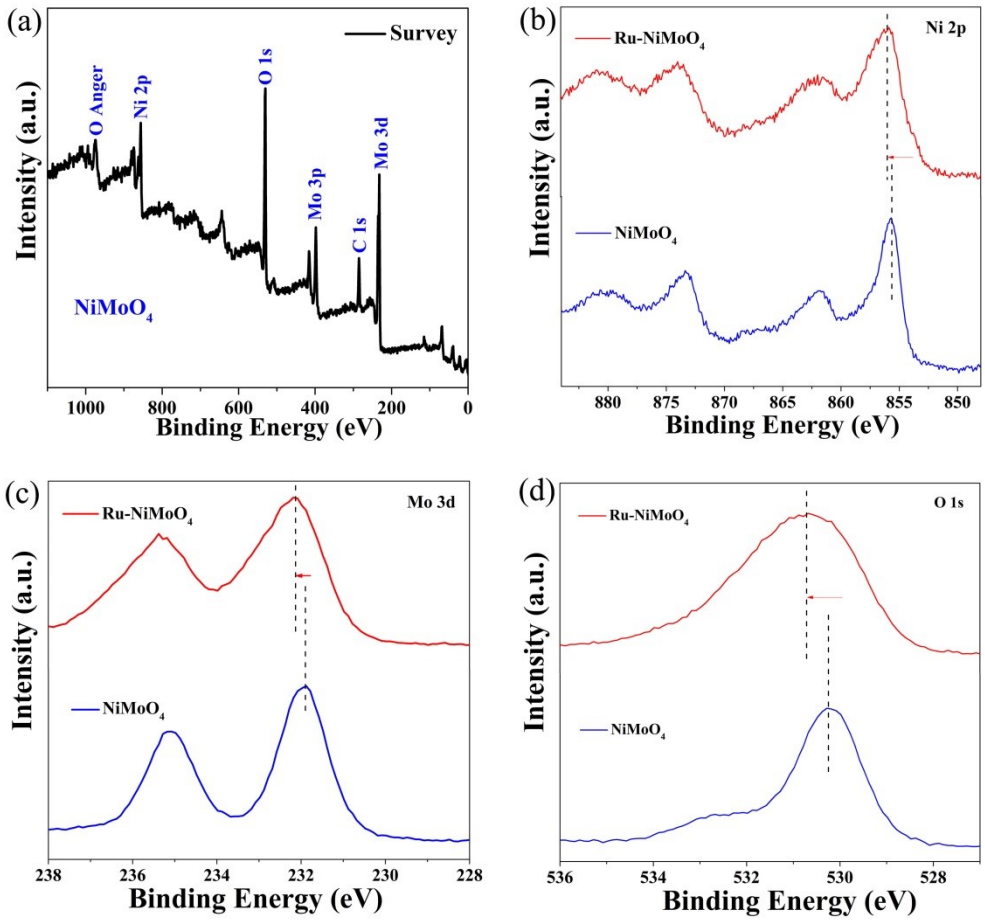

Fig. S5 (a) Full XPS spectrum of $NiMoO_4$-NF. High-resolution XPS spectra of (b) Ni 2p, (c) Mo 3d, and (d) O 1s for $NiMoO_4$-NF and Ru-$NiMoO_4$-NF.

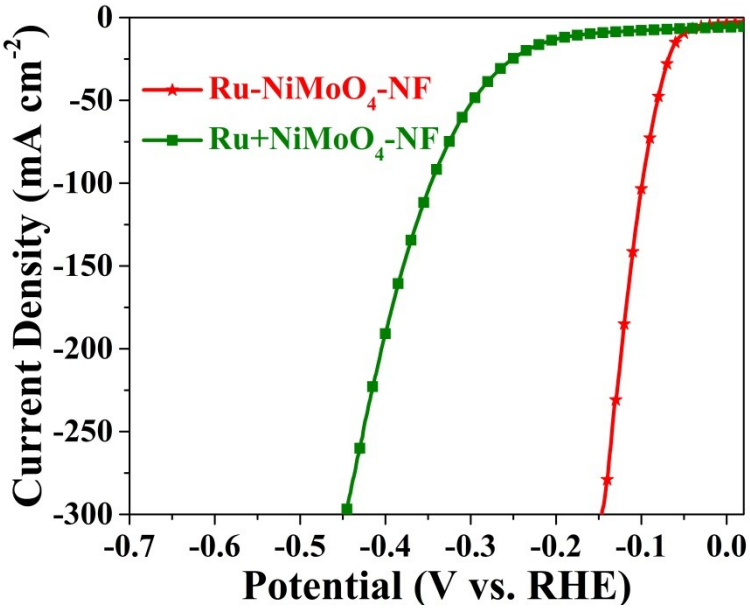

Fig. S6 LSV curves of Ru+$NiMoO_4$-NF and Ru-$NiMoO_4$-NF in 1 mol/L KOH.

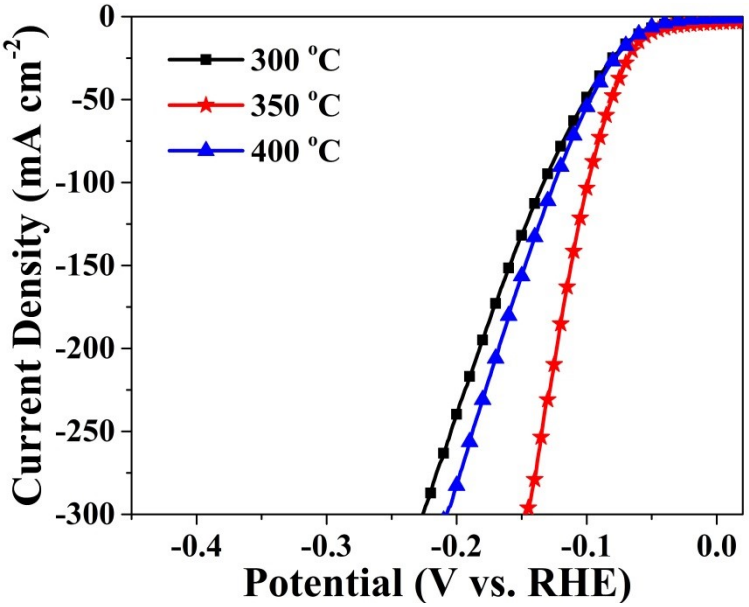

Fig. S7 LSV curves of Ru-$NiMoO_4$-NF at different calcination temperature in 1 mol/L KOH.

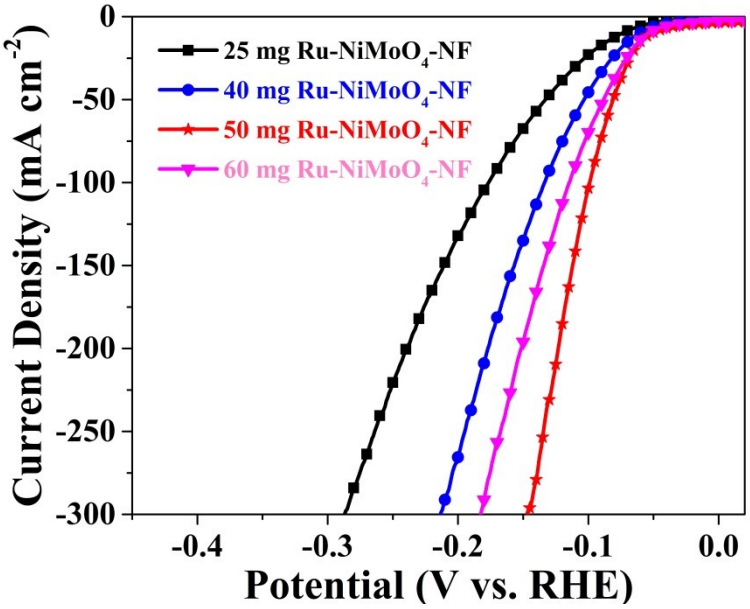

Fig. S8 LSV curves of Ru-$NiMoO_4$-NF with different content of Ru in 1 mol/L KOH.

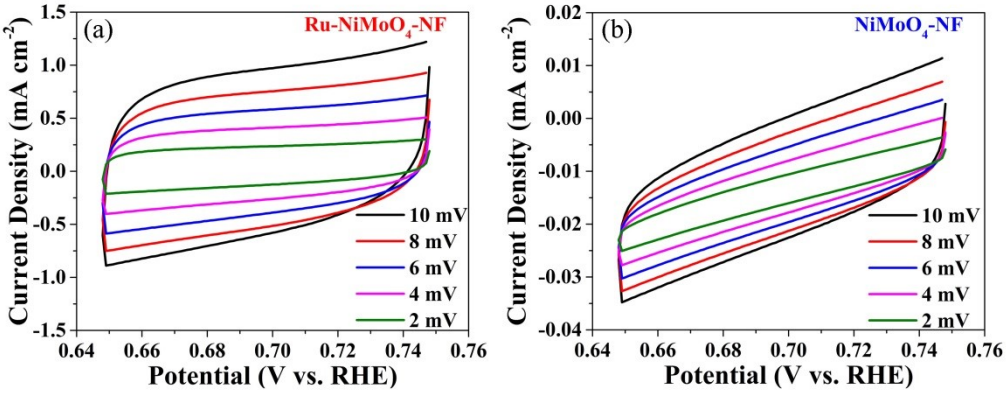

Fig. S9 The cyclic voltammetry curves of (a) Ru-$NiMoO_4$-NF and (b) $NiMoO_4$-NF in 1.0 M KOH recorded at different scan rates from 2 to 10 mV s^{-1}.

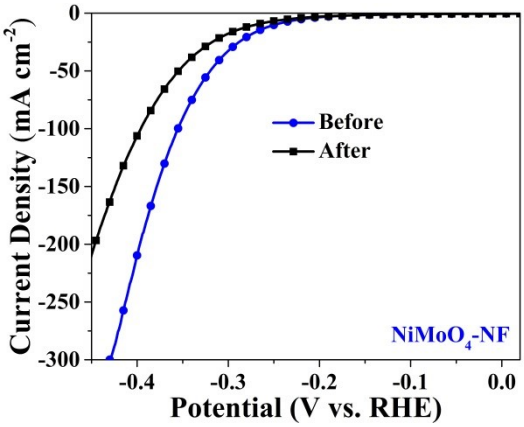

Fig. S10 Polarization curves of $NiMoO_4$-NF before and after 3000 cyclic voltammetry cycles test.

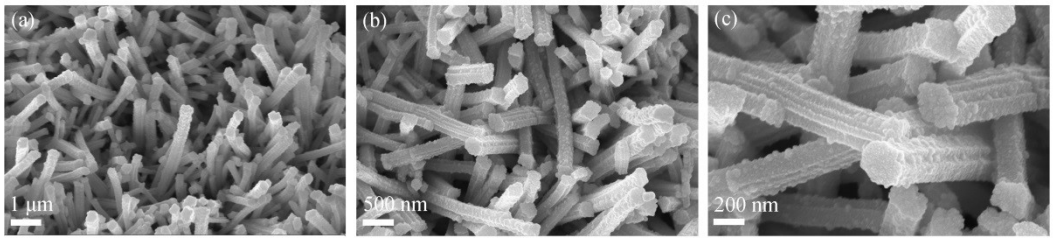

Fig. S11 SEM images of Ru-$NiMoO_4$-NF in alkaline KOH after durability test.

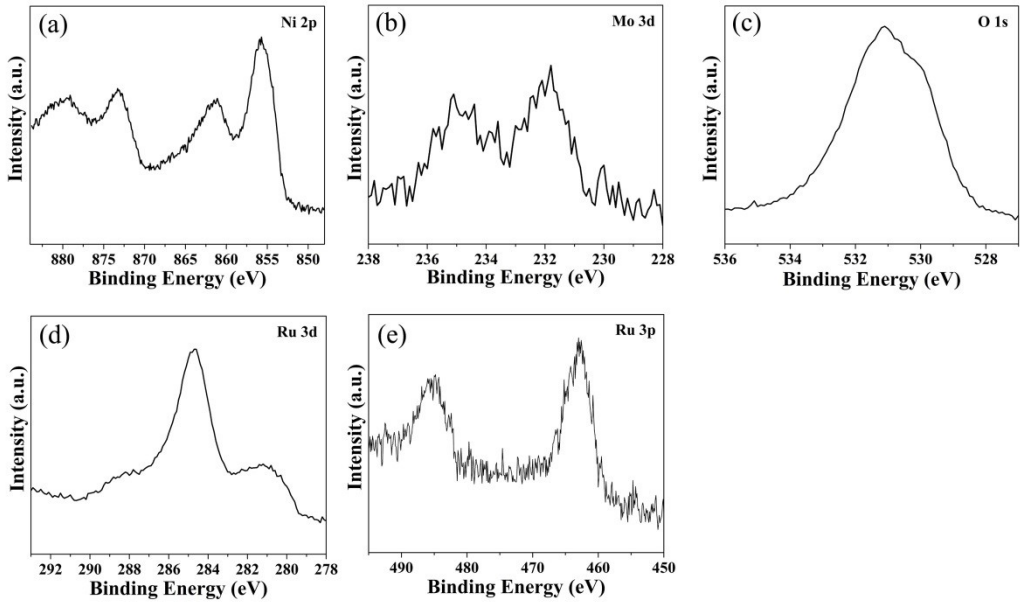

Fig. S12 (a) Ni 2p, (b) Mo 3d, (c) O 1s, (d) Ru 3d, and (e) Ru 3p XPS spectra of Ru-$NiMoO_4$-NF after HER.

Table S1 Comparing the HER activity of our catalysts with other reported $NiMoO_4$-NF electrocatalysts on basis of overpotential at 10 mA cm^{-2} and Tafel slope.

Catalyst	Overpotential at 10 mA cm^{-2}	Tafel slope (mV dec^{-1})	Reference
Ru-$NiMoO_4$-NF	52	45	This work
$NiMoO_4$@Co_3O_4	120	58	[1]
Ru/P-$NiMoO_4$@NF	--	89.2	[2]
Sea urchin-like $NiMoO_4$-200/NF	68	91.33	[3]
RuO_2-NiMoO-CC-30	37	61	[4]
N-$NiMoO_4$/NiS_2	99	74.2	[5]
NiMo HNRs/TiM	92	78	[6]
NiMoN	109	95	[7]
NiMo-NGTs	65	67	[8]
Ni-Mo nanopower	80	--	[9]

Reference

1. G. Solomon, A. Landström, R. Mazzaro, M. Jugovac, P. Moras, E. Cattaruzza, V. Morandi, I. Concina and A. Vomiero, NiMoO4@ Co3O4 core–shell nanorods: in situ catalyst reconstruction toward high efficiency oxygen evolution reaction, *Adv. Energy Mater.*, 2021, **11**, 2101324.
2. L. Guo, J. Chi, J. Zhu, T. Cui, J. Lai and L. Wang, Dual-doping $NiMoO_4$ with multi-channel structure enable urea-assisted energy-saving H_2 production at large current density in alkaline seawater, *Appl. Catal. B: Environ.*, 2023, **320**, 121977.
3. C. Chen, S. He, K. Dastafkan, Z. Zou, Q. Wang and C. Zhao, Sea urchin-like NiMoO4 nanorod arrays as highly efficient bifunctional catalysts for electrocatalytic/photovoltage-driven urea electrolysis, *Chinese Journal of Catalysis*, 2022, **43**, 1267-1276.
4. Z. Zhang, H. Wang, M. Ma, H. Liu, Z. Zhang, W. Zhou and H. Liu, Integrating NiMoO wafer as a heterogeneous 'turbo'for engineering robust Ru-based electrocatalyst for overall water splitting, *Chem. Eng. J.*, 2021, **420**, 127686.
5. L. An, J. Feng, Y. Zhang, R. Wang, H. Liu, G.-C. Wang, F. Cheng and P. Xi, Epitaxial heterogeneous interfaces on N-$NiMoO_4$/NiS_2 nanowires/nanosheets to boost hydrogen and oxygen production for overall water splitting, *Adv. Funct. Mater.*, 2019, **29**, 1805298.

6. J. Tian, N. Cheng, Q. Liu, X. Sun, Y. He and A. M. Asiri, Self-supported NiMo hollow nanorod array: an efficient 3D bifunctional catalytic electrode for overall water splitting, *J. Mater. Chem. A*, 2015, **3**, 20056-20059.
7. Y. Zhang, B. Ouyang, J. Xu, S. Chen, R. S. Rawat and H. J. Fan, 3D porous hierarchical nickel‐molybdenum nitrides synthesized by RF plasma as highly active and stable hydrogen‐evolution‐reaction electrocatalysts, *Adv. Energy Mater.*, 2016, **6**, 1600221.
8. T. Wang, Y. Guo, Z. Zhou, X. Chang, J. Zheng and X. Li, Ni–Mo nanocatalysts on N-doped graphite nanotubes for highly efficient electrochemical hydrogen evolution in acid, *ACS Nano*, 2016, **10**, 10397-10403.
9. J. R. McKone, B. F. Sadtler, C. A. Werlang, N. S. Lewis and H. B. Gray, Ni–Mo nanopowders for efficient electrochemical hydrogen evolution, *ACS Catal.*, 2013, **3**, 166-169.